NUMERICAL MATHEMATICS: Theory, Methods and Applications
Numer. Math. Theor. Meth. Appl., Vol. **xx**, No. x, pp. 1-20 (2019)

An adaptive hybrid spectral method for stochastic Helmholtz problems

Guanjie Wang and Qifeng Liao*

School of Information Science and Technology, ShanghaiTech University, Shanghai, China.

Abstract. The implementation of an adaptive hybrid spectral method for Helmholtz equations with random parameters is addressed in this work. New error indicators for generalized polynomial chaos for stochastic approximations and spectral element methods for physical approximations are developed, and systematic adaptive strategies are proposed associated with these error indicators. Numerical results show that these error indicators provide effective estimates for the approximation errors, and the overall adaptive procedure results in efficient approximation method for the stochastic Helmholtz equations.

AMS subject classifications: 65C30, 65F08, 65N30, 35J05

Key words: Uncertainty quantification, generalized polynomial chaos, spectral elements, Helmholtz equations.

*Corresponding author. *Email addresses:* wanggj@shanghaitech.edu.cn (Guanjie Wang), liaoqf@shanghaitech.edu.cn (Qifeng Liao)

1. Introduction

During the last decade there has been a rapid development in efficient stochastic Galerkin approximation methods for solving partial differential equations (PDEs) with random parameters. The efficiency of Galerkin methods relies on properly choosing basis functions of finite dimensional projection spaces. There are two projection spaces involved herein: the stochastic approximation space and the physical approximation space. In the literature, a popular choice for the stochastic approximation is generalized polynomial chaos (gPC) [18, 37, 39], which is a stochastic spectral method.

Typical choices for the physical approximation are finite element methods [4, 13], spectral methods [8, 32] and spectral element methods [30]. When the solution is sufficiently regular, spectral methods have exponential convergence rates. However, if the solution is not smooth, the rates of spectral methods deteriorate. To result in an efficient approximation in general case, adaptive versions of spectral methods are actively developed.

To resolve discontinuities of solutions with respect to the random parameters, the multi-element generalized polynomial chaos method is first developed [36]. After that, a model reduction based mesh refinement method for stochastic approximations is proposed [28, 29]. For an overall adaptive procedure, adaptive stochastic Galerkin finite element methods are developed in [10], where the gPC degree and dimension adaption and the finite element mesh refinement for the physical domain are conducted based on a residual-based a posteriori error estimator. For efficient adaptive procedures, effective local problem based error estimators for stochastic Galerkin finite elements are developed in [2, 3].

As spectral methods are expected to have higher order accuracy than low order finite element methods, in this work, we develop a new adaptive hybrid spectral method as an alternative to the adaptive stochastic Galerkin finite elements. In this hybrid spectral method, the stochastic domain is discretized by gPC and the physical domain is discretized by the spectral element method, which gives flexibility to conduct local refinements. Since gPC and the (physical) spectral element are both spectral methods, they are both expected to have high order convergence rates. The novelty of this work lies on new effective error indicators and adaptive strategies for both gPC degree adaption and spectral element refinement.

To illustrate the framework and the efficiency of our new approach, the stochastic Helmholtz equations are studied as a benchmark problem, which plays an important role in ocean acoustics, optics and electromagnetics [21,24,42]. The random sources of Helmholtz problems typically arise from lack of knowledge or measurement of material refractive indices or wave number parameters. This paper is organized as follows. In Section 2, the detailed setting of stochastic Helmholtz equations is introduced, and the frameworks of stochastic Galerkin methods and gPC are discussed. We also discuss the spectral element methods for physical approximations in Section 2. Our main adaptive hybrid spectral methods for both stochastic and physical approximations are presented in Section 3. Numerical results are discussed in Section 4. Section 5 concludes the paper.

2. Problem setting and generalized polynomial chaos (gPC)

This section describes the mathematical setting of stochastic Helmholtz equations, its variational formulation, and gPC approximations in the stochastic space.

2.1. Problem setting

Let $D \subset \mathbb{R}^2$ be a physical domain which is open, bounded, connected and with a polygonal boundary ∂D, and $\boldsymbol{x} = [x_1, x_2]^T \in \mathbb{R}^2$ denote a physical variable. Let $\boldsymbol{\xi} = [\xi_1, \ldots, \xi_n]^T$ be a random vector, in which the random variables $\xi_1, \ldots, \xi_n$ are independently distributed on the intervals $\Gamma_1, \ldots, \Gamma_n$. The probability density functions of $\xi_1, \ldots, \xi_n$ are $\pi_1(\xi_1), \ldots, \pi_n(\xi_n)$ respectively. It is clear that the image and the probability density function of $\boldsymbol{\xi}$ are $\Gamma = \Gamma_1 \times \cdots \times \Gamma_n$ and $\pi(\boldsymbol{\xi}) = \pi_1(\xi_1) \cdots \pi_n(\xi_n)$.

In this paper, we consider the transverse electric (TE) polarization for uncertainty in materials, i.e., the following stochastic Helmholtz problem: find the unknown function $u(\boldsymbol{x}, \boldsymbol{\xi})$ satisfying

$$-\nabla^2 u(\boldsymbol{x}, \boldsymbol{\xi}) - \kappa^2(\boldsymbol{x}, \boldsymbol{\xi}) u(\boldsymbol{x}, \boldsymbol{\xi}) = f(\boldsymbol{x}),\ \forall (\boldsymbol{x}, \boldsymbol{\xi}) \in D \times \Gamma, \tag{2.1}$$

$$u(\boldsymbol{x}, \boldsymbol{\xi}) = 0,\ \forall (\boldsymbol{x}, \boldsymbol{\xi}) \in \partial D_{\mathrm{D}} \times \Gamma, \tag{2.2}$$

$$\frac{\partial u}{\partial \boldsymbol{n}} - \mathbf{i}\kappa(\boldsymbol{x}, \boldsymbol{\xi}) u = 0,\ \forall (\boldsymbol{x}, \boldsymbol{\xi}) \in \partial D_{\mathrm{R}} \times \Gamma, \tag{2.3}$$

where $\kappa(\boldsymbol{x}, \boldsymbol{\xi})$ takes values in $\mathbb{R}$; $\mathbf{i} = \sqrt{-1}$, $\partial u / \partial \boldsymbol{n}$ is the outward normal derivative of u, and $\partial D = \partial D_{\mathrm{D}} \cup \partial D_{\mathrm{R}}$ is the boundary of D. As the Karhunen-Loève (KL) expansion is widely used to parameterize random fields [11, 18], we assume $\kappa(\boldsymbol{x}, \boldsymbol{\xi})$ in (2.1) has the same form as the standard KL expansion, i.e.,

$$\kappa(\boldsymbol{x}, \boldsymbol{\xi}) = \sum_{m=0}^{n} \kappa_m(\boldsymbol{x}) \xi_m,$$

where $\{\kappa_m(\boldsymbol{x})\}_{m=0}^n$ are real-valued deterministic functions, and we set $\xi_0 = 1$ for convenience.

To ensure the well-posedness of this problem, we assume that there is a constant $\epsilon > 0$ such that $\kappa(\boldsymbol{x}, \boldsymbol{\xi}) > \epsilon$ for all $(\boldsymbol{x}, \boldsymbol{\xi}) \in D \times \Gamma$, and the eigenvalues associated with deterministic versions of (2.1) are greater than ϵ in magnitude. Thus for each realization of $\boldsymbol{\xi}$ we consider the following deterministic Helmholtz eigenvalue problem — cf. [16, 22, 23]:

$$-\nabla^2 u(\boldsymbol{x}, \boldsymbol{\xi}) - \kappa^2(\boldsymbol{x}, \boldsymbol{\xi}) u(\boldsymbol{x}, \boldsymbol{\xi}) = \lambda(\boldsymbol{\xi}) u(\boldsymbol{x}, \boldsymbol{\xi}) \tag{2.4}$$

with the boundary conditions (2.2)–(2.3). We define a set $\Lambda_{\boldsymbol{\xi}}$ consisting of all eigenvalues of (2.4) for each realization of $\boldsymbol{\xi}$, and assume that $|\lambda| > \epsilon$ for all $\lambda \in \cup_{\boldsymbol{\xi} \in \Gamma} \Lambda_{\boldsymbol{\xi}}$.

2.2. The variational formulation

To introduce the variational form of (2.1)–(2.3), some notation are required. Letting $g(\boldsymbol{\xi})$ be a function of the random vector $\boldsymbol{\xi}$, which maps Γ to $\mathbb{C}$, its expectation (mean value) is defined by

$$\mathbb{E}[g(\boldsymbol{\xi})] := \int_{\Gamma} \pi(\boldsymbol{\xi}) g(\boldsymbol{\xi}) \, \mathrm{d}\boldsymbol{\xi},$$

where $\pi(\boldsymbol{\xi})$ is the probability density function of $\boldsymbol{\xi}$. Next, the Hilbert spaces $L^2(D)$ and $L^2_\pi(\Gamma)$ are defined as

$$L^2(D) := \left\{ v(\boldsymbol{x}) : D \to \mathbb{R} \;\middle|\; \int_D \bar{v} v \, \mathrm{d}\boldsymbol{x} < \infty \right\},$$
$$L^2_\pi(\Gamma) := \left\{ g(\boldsymbol{\xi}) : \Gamma \to \mathbb{R} \;\middle|\; \int_\Gamma \pi(\boldsymbol{\xi}) \bar{g} g \, \mathrm{d}\boldsymbol{\xi} < \infty \right\},$$

which are equipped with the inner products

$$(\hat{v}(\boldsymbol{x}), v(\boldsymbol{x}))_{L^2(D)} := \int_D \bar{v}(\boldsymbol{x}) \hat{v}(\boldsymbol{x}) \, \mathrm{d}\boldsymbol{x},$$
$$(\hat{g}(\boldsymbol{\xi}), g(\boldsymbol{\xi}))_{L^2_\pi(\Gamma)} := \int_\Gamma \pi(\boldsymbol{\xi}) \bar{g}(\boldsymbol{\xi}) \hat{g}(\boldsymbol{\xi}) \, \mathrm{d}\boldsymbol{\xi}.$$

Following Babuška [1], we define the tensor space of $L^2(D)$ and $L^2_\pi(\Gamma)$ as

$$\begin{aligned} &L^2(D) \otimes L^2_\pi(\Gamma) \\ &:= \left\{ w(\boldsymbol{x}, \boldsymbol{\xi}) \middle| w(\boldsymbol{x}, \boldsymbol{\xi}) = \sum_{i=1}^{n} v_i(\boldsymbol{x}) g_i(\boldsymbol{\xi}), v_i(\boldsymbol{x}) \in L^2(D),\ g_i(\boldsymbol{\xi}) \in L^2_\pi(\Gamma), n \in \mathbb{N}^+ \right\}, \end{aligned}$$

which is equipped with the tensor inner product

$$(\hat{w}(\boldsymbol{x}, \boldsymbol{\xi}), w(\boldsymbol{x}, \boldsymbol{\xi}))_{L^2(D) \otimes L^2_\pi(\Gamma)} = \mathbb{E}\left[\int_D \bar{w}(\boldsymbol{x}, \boldsymbol{\xi}) \hat{w}(\boldsymbol{x}, \boldsymbol{\xi}) \, \mathrm{d}\boldsymbol{x} \right].$$

Following [15, 31, 39], the variational form of (2.1)–(2.3) can be written as: find $u \in W := L^2(D) \otimes L^2_\pi(\Gamma)$, such that

$$\mathbb{E}\left[\int_D \nabla u \cdot \nabla \bar{w} - \int_D \kappa^2 u \bar{w} - \mathbf{i} \int_{\partial D_{\mathrm{R}}} \kappa u \bar{w} \right] = \mathbb{E}\left[\int_D f \bar{w} \right], \ \forall w \in W. \tag{2.5}$$

Ihlenburg and Babuška [19, 20] show that the variational problem associated with the deterministic Helmholtz equations has a unique solution and establish a priori error estimates for the corresponding finite element methods. After that, Cao *et al.* [5] prove that the variational problem associated with Helmholtz equations with discretized white noise forcing term has a unique solution and provide a priori error estimates for the corresponding finite

element and discontinuous Galerkin methods. In this work, we focus on the situation that there exist uncertainties in the coefficient κ.

Since the stochastic space $L^2_\pi(\Gamma)$ and the physical space $L^2(D)$ are independent to each other, we discretize the stochastic and physical spaces independently, i.e., choosing the finite-dimensional subspaces of them respectively, and then take the tensor space of these subspaces as the finite-dimensional subspace of $W = L^2(D) \otimes L^2_\pi(\Gamma)$. In general, let

$$\mathscr{V}_{\text{phy}} = \text{span}\{v_i(\boldsymbol{x}),\ i = 1, \ldots, N_{\boldsymbol{x}}\}$$

and

$$\mathscr{V}_{\text{stoch}} = \text{span}\{\Phi_j(\boldsymbol{\xi}),\ j = 1, \ldots\ N_{\boldsymbol{\xi}}\}$$

denote finite-dimensional subspaces of $L^2(D)$ and $L^2_\pi(\Gamma)$. The tensor space of them, i.e.,

$$\mathscr{V}_{\text{phy}} \otimes \mathscr{V}_{\text{stoch}} = \{v_i(\boldsymbol{x})\Phi_j(\boldsymbol{\xi}),\ i = 1, \ldots, N_{\boldsymbol{x}},\ j = 1, \ldots, N_{\boldsymbol{\xi}}\}$$

is taken as the finite-dimensional subspace of W. Thus, we have

$$u(\boldsymbol{x}, \boldsymbol{\xi}) \approx u_{\text{ap}}(\boldsymbol{x}, \boldsymbol{\xi}) := \sum_{j=1}^{N_{\boldsymbol{\xi}}} \sum_{i=1}^{N_{\boldsymbol{x}}} u_{ji} v_i(\boldsymbol{x}) \Phi_j(\boldsymbol{\xi}). \tag{2.6}$$

Substitute (2.6) to the variational form (2.5), we obtain the linear system

$$\boldsymbol{A}\boldsymbol{u} = \boldsymbol{b}, \tag{2.7}$$

where

$$\boldsymbol{A} = \boldsymbol{G}_{00} \otimes \boldsymbol{K} - \sum_{l=0}^{n} \sum_{m=0}^{n} \boldsymbol{G}_{lm} \otimes \boldsymbol{M}_{lm} - \sum_{l=0}^{n} \mathbf{i}\boldsymbol{G}_{l0} \otimes \boldsymbol{L}_l; \tag{2.8}$$

$$\boldsymbol{b} = \boldsymbol{h} \otimes \boldsymbol{f}. \tag{2.9}$$

In (2.8)–(2.9), $\otimes$ denotes Kronecker tensor product and

$$\boldsymbol{h}(j) = \mathbb{E}\big[\Phi_j(\boldsymbol{\xi})\big],\ \boldsymbol{f}(s) = \int_D f\, v_s \,\mathrm{d}\boldsymbol{x},$$

$$\boldsymbol{M}_{lm}(s,t) = \int_D \kappa_l \kappa_m v_s v_t \,\mathrm{d}\boldsymbol{x},\ \boldsymbol{L}_l(s,t) = \int_{\partial D_{\text{R}}} \kappa_l v_s v_t \,\mathrm{d}s,$$

$$\boldsymbol{G}_{lm}(j,k) = \mathbb{E}\big[\xi_l \xi_m \Phi_j(\boldsymbol{\xi})\Phi_k(\boldsymbol{\xi})\big],\ \boldsymbol{K}(s,t) = \int_D \nabla v_s \cdot \nabla v_t \,\mathrm{d}\boldsymbol{x},$$

where $l, m = 0, 1, \ldots, n$; $j, k = 1, \ldots, N_{\boldsymbol{\xi}}$ and $s, t = 1, \ldots, N_{\boldsymbol{x}}$.

2.3. The generalized polynomial chaos expansion

There are two main kinds of bases for the stochastic space, i.e., the piecewise linear functions and the global orthogonal polynomials. The former achieves a desired accuracy through polynomial approximation with a fixed degree on an increasingly fine partition of Γ [1,9]. The later one reduces the error via increasing the degrees of polynomial bases. It includes polynomial chaos [17,18], generalized polynomial chaos [14,40] and dynamically bi-orthogonal polynomials [6,7,27,44]. In this work, we use the generalised polynomial chaos approximation in stochastic space. For completeness we review the generalized polynomial chaos expansion following [37,38,40].

The generalized polynomial chaos (gPC) expansion is widely used to represent stochastic processes. By gPC expansion, $u(\boldsymbol{x},\boldsymbol{\xi})$ can be expressed as [41]

$$u(\boldsymbol{x},\boldsymbol{\xi}) := \sum_{|\boldsymbol{j}|=0}^{\infty} u_{\boldsymbol{j}}(\boldsymbol{x})\Phi_{\boldsymbol{j}}(\boldsymbol{\xi}), \tag{2.10}$$

where $\boldsymbol{j} = (j_1,\ldots,j_n)$ is a multi-index with $|\boldsymbol{j}| = j_1 + \ldots + j_n$, $\{\Phi_{\boldsymbol{j}}(\boldsymbol{\xi})\}_{|\boldsymbol{j}|=0}^{\infty}$ consists of n-variate $|j|$-th order orthogonal polynomials with respect to the inner product $(\cdot,\cdot)_{L^2_\pi}$, which are named as the generalized polynomial chaos, and each $u_{\boldsymbol{j}}(\boldsymbol{x}) := \int_\Gamma u(\boldsymbol{x},\boldsymbol{\xi})\Phi_{\boldsymbol{j}}(\boldsymbol{\xi})d\boldsymbol{\xi}$ is a gPC coefficient function. The generalized polynomial chaos can be expressed by the products of a sequence of univariate polynomials in each direction of $\boldsymbol{\xi}$ when $\xi_1,\ldots,\xi_n$ are independent, i.e.,

$$\Phi_{\boldsymbol{j}}(\boldsymbol{\xi}) = \phi_{j_1}(\xi_1)\cdots\phi_{j_n}(\xi_n),$$

where j_i $(1 \le i \le n)$ are the degrees of the univariate polynomial $\phi_{j_i}(\xi_i)$, and $\{\phi_{j_i}(\xi_i)\}$ are orthonormal polynomials with respect to $\pi_i(\xi_i)$, i.e.,

$$\int_{\Gamma_i} \pi(\xi_i)\phi_{j_i}(\xi_i)\phi_{k_i}(\xi_i)\mathrm{d}\xi_i = \delta_{j_i,k_i}. \tag{2.11}$$

In (2.11), δ_{j_i,k_i} is the Kronecker delta function and $\pi_i(\xi_i)$ is the probability density function of ξ_i.

It follows immediately form (2.11) that

$$\mathbb{E}\big[\Phi_{\boldsymbol{j}}(\boldsymbol{\xi})\Phi_{\boldsymbol{k}}(\boldsymbol{\xi})\big] = \int_\Gamma \pi(\boldsymbol{\xi})\Phi_{\boldsymbol{j}}(\boldsymbol{\xi})\Phi_{\boldsymbol{k}}(\boldsymbol{\xi}) = \delta_{\boldsymbol{j},\boldsymbol{k}}, \tag{2.12}$$

where $\delta_{\boldsymbol{j},\boldsymbol{k}} = \delta_{j_1,k_1}\cdots\delta_{j_n,k_n}$.

From (2.12), the mean and variance of $u(\boldsymbol{x},\boldsymbol{\xi})$ are given by

$$\mathbb{E}[u(\boldsymbol{x},\boldsymbol{\xi})] = u_{\boldsymbol{0}}(\boldsymbol{x}),\ \mathbb{V}[u(\boldsymbol{x},\boldsymbol{\xi})] = \sum_{|\boldsymbol{j}|=1}^{\infty} u_{\boldsymbol{j}}^2(\boldsymbol{x}).$$

Truncating the gPC expansion (2.10) up to degree q, we get a q-th order gPC approximation of $u(\boldsymbol{x},\boldsymbol{\xi})$, i.e.,

$$u(\boldsymbol{x},\boldsymbol{\xi}) \approx \sum_{|\boldsymbol{j}|=0}^{q} u_{\boldsymbol{j}}(\boldsymbol{x})\Phi_{\boldsymbol{j}}(\boldsymbol{\xi}).$$

For the q-th order gPC approximation, the finite-dimension subspace of $L^2_\pi(\Gamma)$ is

$$\mathscr{V}_{\text{stoch}} := \mathscr{P}_q^n(\boldsymbol{\xi}) = \text{span}\{\Phi_{\boldsymbol{j}}(\boldsymbol{\xi}),\ |\boldsymbol{j}| \le q\},$$

and it is clear that $\{\Phi_{\boldsymbol{j}}(\boldsymbol{\xi})\}_{|\boldsymbol{j}|\le q}$ is the basis of $\mathscr{P}_q^n(\boldsymbol{\xi})$.

2.4. The spectral element method in physical space

For the spatial point of view, we use the spectral element method (SEM) to discretize the physical domain [30]. Like the finite element methods, we first divide the physical domain D into non-overlapping elements:

$$\bigcup_{m=1}^{N_D} \bar{D}_m = \bar{D},\ \ D_m \bigcap D_m = \emptyset,\ \text{for } m \ne n,$$

where N_D is the number of elements. Then the approximation space can be taken as

$$\mathscr{V}_{\text{phy}} := \mathscr{V}_p^h = \{v \in L^2(D) \Big| v|_{D_m} \in P_p(D_m)\},$$

where $P_p(D_m)$ denotes the polynomials in D_m with maximum degrees not greater than p. In this paper, quadrilateral elements are used to divide the physical domain D.

It is known that each quadrilateral element D_m can be transformed to the reference element $(s,t) \in D_{\text{r}} := [-1,1]\times[-1,1]$ by changing variables through an isoparametric transformation [13]. The discrete points and basis functions on element D_m can be obtained by mapping the points and basis functions on the reference element D_{r} to D_m through the isoparametric transformation. Since all computations are implemented on the reference element, the basis functions on element D_m need not be formulated explicitly.

On the reference element, the discrete points and basis functions are the tensor product of the discrete points and basis functions in each direction. Supposing $-1 = s_0 < s_1 < \cdots < s_p = 1$ are the discrete points in $[-1,1]$, the basis functions in $[-1,1]$ are p-th order Lagrange interpolation polynomials through the points. That is

$$l_j(s) = l(s)\frac{\lambda_j}{s-s_j},$$

where

$$l(s) = \prod_{j=0}^{p}(s-s_j),\ \lambda_j = \frac{1}{l'(s_j)} = \frac{1}{\prod_{j\ne k}(s_j-s_k)}.$$

It is clear that, the basis functions in $[-1,1]$, i.e., the Lagrange interpolation polynomials, satisfy

$$l_j(s_i) = \delta_{i,j}.$$

It is known that for equally spaced points, the p-th order Lagrange interpolation in $[-1,1]$ is unstable as p increases, which is called the Runge phenomenon. The interpolation

becomes stable if the interpolate points are moved to Gauss-Lobatto points, which consist of the end-points ± 1 and the extreme points of a p-th degree orthogonal polynomial in $[-1,1]$, for example, the Legendre-Gauss-Lobatto (LGL) points [32] which include the extreme points of Legendre polynomials and ± 1, and the Chebyshev-Gauss-Lobatto (CGL) points [33] which consist of the extreme points of Chebyshev polynomial and ± 1. For CGL points, there is an explicit formula:

$$s_i = \cos((p-i)\pi/p), \quad i = 0, 1, \ldots, p.$$

Moreover, the barycentric weights for CGL points are $\lambda_j = (-1)^j$, but the terms of $j = 0$ and $j = p$ should be multiplied by $1/2$. Thus we choose the discrete points based on CGL points in this paper.

Once the points and basis functions in $[-1,1]$ are determined, the discrete points and basis functions on the reference element D_{r} can be obtained by applying the tensor product of each direction. Cf. [30, 35] for details.

3. The adaptive procedure

For the stochastic Galerkin method, there are two sources of truncation errors, i.e., the errors from physical and stochastic approximations. More precisely, the square of overall errors can be written as:

$$\begin{aligned}&\|u(\boldsymbol{x},\boldsymbol{\xi}) - u_{\mathrm{ap}}(\boldsymbol{x},\boldsymbol{\xi})\|^2_{L^2(D)\otimes L^2_\pi(\Gamma)}\\ =&\|u(\boldsymbol{x},\boldsymbol{\xi}) - u^q(\boldsymbol{x},\boldsymbol{\xi}) + u^q(\boldsymbol{x},\boldsymbol{\xi}) - u_{\mathrm{ap}}(\boldsymbol{x},\boldsymbol{\xi})\|^2_{L^2(D)\otimes L^2_\pi(\Gamma)}\end{aligned}$$

where $u^q(\boldsymbol{x},\boldsymbol{\xi}) = \sum_{|\boldsymbol{j}|=0}^{q} u_{\boldsymbol{j}}(\boldsymbol{x})\Phi_{\boldsymbol{j}}(\boldsymbol{\xi})$. Denoting $e_{\boldsymbol{j}}(\boldsymbol{x}) = u_{\boldsymbol{j}}(\boldsymbol{x}) - u^{\mathrm{ap}}_{\boldsymbol{j}}(\boldsymbol{x})$, where $u^{\mathrm{ap}}_{\boldsymbol{j}}(\boldsymbol{x}) := \int_\Gamma u_{\mathrm{ap}}(\boldsymbol{x},\boldsymbol{\xi})\Phi_{\boldsymbol{j}}(\boldsymbol{\xi})d\boldsymbol{\xi} = \sum_{i=1}^{N_{\boldsymbol{x}}} u_{\boldsymbol{j}i}v_i(\boldsymbol{x})$ (see (2.6)), we have

$$\begin{aligned}u^q(\boldsymbol{x},\boldsymbol{\xi}) - u_{\mathrm{ap}}(\boldsymbol{x},\boldsymbol{\xi}) &= \sum_{|\boldsymbol{j}|=0}^{q} e_{\boldsymbol{j}}(\boldsymbol{x})\Phi_{\boldsymbol{j}}(\boldsymbol{\xi}),\\ u(\boldsymbol{x},\boldsymbol{\xi}) - u^q(\boldsymbol{x},\boldsymbol{\xi}) &= \sum_{|\boldsymbol{j}|=q+1}^{\infty} u_{\boldsymbol{j}}(\boldsymbol{x})\Phi_{\boldsymbol{j}}(\boldsymbol{\xi}).\end{aligned}$$

Since $\{\Phi_{\boldsymbol{j}}(\boldsymbol{\xi})\}$ are orthonormal basis functions for stochastic approximation, the terms $e_{\boldsymbol{j}}(\boldsymbol{x})\Phi_{\boldsymbol{j}}(\boldsymbol{\xi})$ with $|\boldsymbol{j}| \le q$ and the terms $u_{\boldsymbol{j}}(\boldsymbol{x})\Phi_{\boldsymbol{j}}$ with $|\boldsymbol{j}| \ge q+1$ are orthogonal. Thus we have

$$\begin{aligned}&\|u(\boldsymbol{x},\boldsymbol{\xi}) - u_{\mathrm{ap}}(\boldsymbol{x},\boldsymbol{\xi})\|^2_{L^2(D)\otimes L^2_\pi(\Gamma)}\\ =&\|u(\boldsymbol{x},\boldsymbol{\xi}) - u^q(\boldsymbol{x},\boldsymbol{\xi})\|^2_{L^2(D)\otimes L^2_\pi(\Gamma)} + \|u^q(\boldsymbol{x},\boldsymbol{\xi}) - u_{\mathrm{ap}}(\boldsymbol{x},\boldsymbol{\xi})\|^2_{L^2(D)\otimes L^2_\pi(\Gamma)}\\ =&\|\sum_{|\boldsymbol{j}|=q+1}^{\infty} u_{\boldsymbol{j}}(\boldsymbol{x})\Phi_{\boldsymbol{j}}(\boldsymbol{\xi})\|^2_{L^2(D)\otimes L^2_\pi(\Gamma)} + \|\sum_{|\boldsymbol{j}|=0}^{q} e_{\boldsymbol{j}}(\boldsymbol{x})\Phi_{\boldsymbol{j}}(\boldsymbol{\xi})\|^2_{L^2(D)\otimes L^2_\pi(\Gamma)}\\ =&\sum_{|\boldsymbol{j}|=q+1}^{\infty} \|u_{\boldsymbol{j}}(\boldsymbol{x})\|^2_{L^2(D)} + \sum_{|\boldsymbol{j}|=0}^{q} \|e_{\boldsymbol{j}}(\boldsymbol{x})\|^2_{L^2(D)}.\end{aligned} \tag{3.1}$$

In (3.1), the term $\sum_{|\boldsymbol{j}|=q+1}^{\infty} \|u_{\boldsymbol{j}}(\boldsymbol{x})\|^2_{L^2(D)}$ is the square of the stochastic approximation error, and the term $\sum_{|\boldsymbol{j}|=0}^{q} \|e_{\boldsymbol{j}}(\boldsymbol{x})\|^2_{L^2(D)}$ is the square of the physical approximation error.

Next, the over all relative error is defined as

$$\mathtt{err} := \|u(\boldsymbol{x},\boldsymbol{\xi}) - u_{\mathrm{ap}}(\boldsymbol{x},\boldsymbol{\xi})\|_{L^2(D)\otimes L^2_\pi(\Gamma)} \big/ \|u(\boldsymbol{x},\boldsymbol{\xi})\|_{L^2(D)\otimes L^2_\pi(\Gamma)}. \tag{3.2}$$

That is

$$\mathtt{err} = \left(\mathtt{err}^2_{\mathrm{stoch}} + \mathtt{err}^2_{\mathrm{phy}}\right)^{1/2}, \tag{3.3}$$

where

$$\mathtt{err}^2_{\mathrm{phy}} := \sum_{|\boldsymbol{j}|=0}^{q} \|e_{\boldsymbol{j}}(\boldsymbol{x})\|^2_{L^2(D)} \big/ \|u(\boldsymbol{x},\boldsymbol{\xi})\|^2_{L^2(D)\otimes L^2_\pi(\Gamma)}, \tag{3.4}$$

$$\mathtt{err}^2_{\mathrm{stoch}} := \sum_{|\boldsymbol{j}|=q+1}^{\infty} \|u_{\boldsymbol{j}}(\boldsymbol{x})\|^2_{L^2(D)} \big/ \|u(\boldsymbol{x},\boldsymbol{\xi})\|^2_{L^2(D)\otimes L^2_\pi(\Gamma)}. \tag{3.5}$$

Since

$$\|u^q(\boldsymbol{x},\boldsymbol{\xi})\|^2_{L^2(D)\otimes L^2_\pi(\Gamma)} \le \|u(\boldsymbol{x},\boldsymbol{\xi})\|^2_{L^2(D)\otimes L^2_\pi(\Gamma)},$$

we have

$$\mathtt{err}^2_{\mathrm{phy}} \le \sum_{|\boldsymbol{j}|=0}^{q} \|e_{\boldsymbol{j}}(\boldsymbol{x})\|^2_{L^2(D)} \big/ \|u^q(\boldsymbol{x},\boldsymbol{\xi})\|^2_{L^2(D)\otimes L^2_\pi(\Gamma)},$$

For convenience, we define a symbol $\lesssim$: for $a, b \in \mathbb{R}$, $a \lesssim b$ if and only if $a \le C\,b$ where C is generic constant independent of a and b. As discussed in [39], if the exact solution $u(\boldsymbol{x},\boldsymbol{\xi})$ of (2.5) is analytic with respect to $\boldsymbol{\xi}$, moduli of gPC coefficients decay exponentially as the gPC order increases. The rate of exponential decay depends on the regularity of the solution with respect to $\boldsymbol{\xi}$. Tang and Zhou [43] investigate a stochastic collocation method for scalar hyperbolic equations with a random wave speed and show that the rate of convergence depends on the regularity of solutions. We note that the mean of $u(\boldsymbol{x},\boldsymbol{\xi})$ is $u_{\boldsymbol{0}}(\boldsymbol{x})$ and the variance is $\sum_{|\boldsymbol{j}|>0} u^2_{\boldsymbol{j}}(\boldsymbol{x})$. In this work, we restrict our attention to the situation that the standard deviation of $u(\boldsymbol{x},\boldsymbol{\xi})$ is not much larger than the expectation, and we then assume

$$\|u_{\boldsymbol{j}}\|^2_{L^2(D)} \lesssim \|u_{\boldsymbol{i}}\|^2_{L^2(D)} \text{ for } |\boldsymbol{j}| > 0 \text{ and } |\boldsymbol{i}| = 0.$$

This assumption is true when the variance of $\kappa(\boldsymbol{x},\boldsymbol{\xi})$ is small or when the solution of (2.5) changes modestly with respect to $\boldsymbol{\xi}$. Based on the above assumption, we further assume

$$\|e_{\boldsymbol{j}}\|_{L^2(D)} \lesssim \|e_{\boldsymbol{i}}\|_{L^2(D)} \text{ for } |\boldsymbol{j}| > 0 \text{ and } |\boldsymbol{i}| = 0. \tag{3.6}$$

Note that $\|u^q(\boldsymbol{x},\boldsymbol{\xi})\|^2_{L^2(D)\otimes L^2_\pi(\Gamma)} = \sum_{|\boldsymbol{j}|=0}^{q} \|u_{\boldsymbol{j}}\|^2_{L^2(D)} \ge \|u_{\boldsymbol{0}}(\boldsymbol{x})\|^2_{L^2(D)}$, and we have an upper bound of the error for physical approximation:

$$\mathtt{err}_{\mathrm{phy}} \lesssim \|e_{\boldsymbol{0}}(\boldsymbol{x})\|_{L^2(D)} \big/ \|u_{\boldsymbol{0}}(\boldsymbol{x})\|_{L^2(D)}. \tag{3.7}$$

For spectral element method, there are some strategies to estimate the right hand side of (3.7) [25,26]. In this paper, we estimate the right hand side of (3.7) as following. First, the approximate solution $u_{\mathbf{0}}^{\mathrm{ap}}(\boldsymbol{x})$ is rewritten as

$$u_{\mathbf{0}}^{\mathrm{ap}}(\boldsymbol{x}) = \sum_{m=1}^{N_D} u_{\mathbf{0},m}^{\mathrm{ap}}(F_m(s,t)),\ u_{\mathbf{0},m}^{\mathrm{ap}}(\boldsymbol{x}) = u_{\mathbf{0}}^{\mathrm{ap}}(\boldsymbol{x})|_{D_m},$$

where $(x_1, x_2) = F_m(s,t)$ is the isoparametric transformation from the reference element D_{r} to D_m, $m = 1, \ldots, N_D$.

In the following, we derive an error indicator of each local approximation solution $u_{\mathbf{0},m}^{\mathrm{ap}}$ through its Chebyshev expansion (note that the local solution is obtained through Lagrange polynomial basis as discussed in Section 2.4). On each element D_m, the local solution $u_{\mathbf{0},m}^{\mathrm{ap}}(F_m(s,t))$ can be expanded as the Chebyshev series,

$$u_{\mathbf{0},m}^{\mathrm{ap}}(s,t) := u_{\mathbf{0},m}^{\mathrm{ap}}(F_m(s,t)) = \sum_{i=0}^{p}\sum_{j=0}^{p} a_{ij}^m T_i(s) T_j(t), \tag{3.8}$$

where $\{T_i(\cdot)\}_{i=0}^p$ are Chebyshev polynomials and $\{a_{ij}^m\}_{i,j=0}^p$ are coefficients of the Chebyshev expansion of $u_{\mathbf{0},m}^{\mathrm{ap}}$. In [34], it is proven that if for some $h > 0$, $u_{\mathbf{0},m}^{\mathrm{ap}}(s,t)$ is analytic for all $(s,t) \in \{(\tilde{s},\tilde{t})|\,(\tilde{s},\tilde{t}) \in \mathbb{C}^2,\ \text{and}\ \tilde{s}^2 + \tilde{t}^2 \in N_{2,h^2}\}$ where $N_{2,h^2} := \{\tilde{s}|\,\tilde{s} \in \mathbb{C},\ \text{and}\ |\tilde{s}| + |\tilde{s} - 2| < 2 + 2h^2\}$, then for $\forall\ \epsilon > 0$, we have $|a_{ij}^m| = O((\rho - \epsilon)^{-\sqrt{i^2+j^2}})$, where $\rho = h + \sqrt{1+h^2}$. This implies that the moduli of the coefficients in (3.8) decrease exponentially if the local solution $u_{\mathbf{0},m}^{\mathrm{ap}}(F_m(s,t))$ is analytic. Thus we use

$$\mathtt{err}_{\mathrm{phyest}} := \left(\sum_{m=1}^{N_D} \eta_m^2\right)^{1/2} \Big/ \|u_{\mathbf{0}}^{\mathrm{ap}}(\boldsymbol{x})\|_{L^2(D)}, \tag{3.9}$$

to estimate $\|e_{\mathbf{0}}(\boldsymbol{x})\|_{L^2(D)} \big/ \|u_{\mathbf{0}}(\boldsymbol{x})\|_{L^2(D)}$, where

$$\eta_m = \| \sum_{\max(i,j)=p} a_{ij}^m T_i(s) T_j(t)\|_{L^2(D_m)}.$$

Supposing the tolerance for the physical approximation is denoted by ϵ, the elements with

$$\eta_m > \epsilon \|u_{\mathbf{0}}^{\mathrm{ap}}(\boldsymbol{x})\|_{L^2(D)} \Big/ \sqrt{N_D}$$

need to be split. Note that when $\eta_1 = \ldots = \eta_m = \epsilon \|u_{\mathbf{0}}^{\mathrm{ap}}(\boldsymbol{x})\|_{L^2(D)} \Big/ \sqrt{N_D}$, $\mathtt{err}_{\mathrm{phyest}} = \epsilon$.

Since the contribution of different directions may not be the same, there are three ways to split the elements, and Figure 1 gives the sketch of them. If x_i $(i = 1, 2)$ contributes the main error, the element is only split in x_i direction. If the contributions of two directions

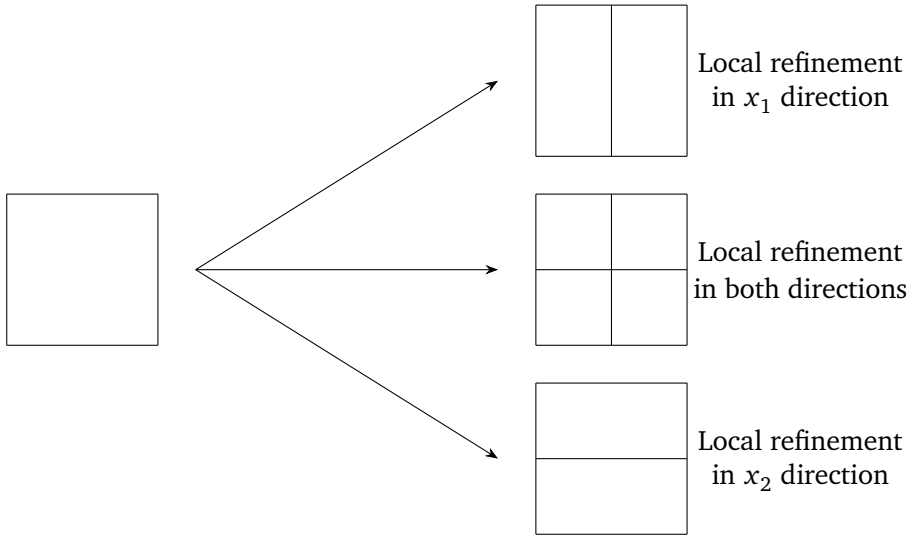

Figure 1: Local refinements for an element.

are nearly the same, the element is split in both directions. More precisely, for the m-th element, the following error indicators are defined:

$$\beta_{m1} = \| \sum_{j=0}^{p} a_{pj}^{m} T_p(s) T_j(t) \|_{L^2(D_m)}, \tag{3.10}$$

$$\beta_{m2} = \| \sum_{i=0}^{p} a_{ip}^{m} T_i(s) T_p(t) \|_{L^2(D_m)}. \tag{3.11}$$

If $\beta_{mi} > 2/3 \max(\beta_{m1}, \beta_{m2})$, the m-th element is split in x_i direction evenly.

To summarize, the physical mesh can be refined by Algorithm 3.1.

Algorithm 3.1 The mesh refinement scheme

Set the tolerance ϵ, and initialize the mesh T.
Compute the numerical solution $u_{\text{ap}}(\boldsymbol{x}, \boldsymbol{\xi})$ in (2.6).
Compute $\{\eta_m\}_{m=1}^{N_D}$, $\{\beta_{mi}\}_{m=1}^{N_D}$ and $\texttt{err}_{\text{phyest}}$ in (3.9)–(3.11).
if $\texttt{err}_{\text{phyest}} > \epsilon$ **then**
  for $m = 1 : N_D$ **do**
    if $\eta_m > \epsilon \|u_{\mathbf{0}}^{\text{ap}}(\boldsymbol{x})\|_{L^2} \Big/ \sqrt{N_D}$ and $\beta_{mi} > 2/3 \max(\beta_{m1}, \beta_{m2})$ **then**
      Split the elements along x_i direction evenly.
    end if
  end for
end if

On the other hand, for the stochastic approximation, we have

$$\mathtt{err}_{\text{stoch}} \leq \left(\sum_{|\boldsymbol{j}|=q+1}^{\infty} \|u_{\boldsymbol{j}}(\boldsymbol{x})\|^2_{L^2(D)} \Big/ \sum_{|\boldsymbol{j}|=1}^{\infty} \|u_{\boldsymbol{j}}(\boldsymbol{x})\|^2_{L^2(D)} \right)^{1/2}. \tag{3.12}$$

Note that the right hand side of (3.12) is exactly the relative error of variance function for gPC expansion with total degree q. Following [36], we estimate this error as

$$\mathtt{err}_{\text{stochest}} = \left(\sum_{|\boldsymbol{j}|=q} \|u^{\text{ap}}_{\boldsymbol{j}}(\boldsymbol{x})\|^2_{L^2(D)} \Big/ \sum_{|\boldsymbol{j}|=1}^{q} \|u^{\text{ap}}_{\boldsymbol{j}}(\boldsymbol{x})\|^2_{L^2(D)} \right)^{1/2}. \tag{3.13}$$

When $\mathtt{err}_{\text{stochest}}$ is greater than the tolerance for the physical approximation, we increase the degree q.

Recalling (3.3), the over all error is

$$\mathtt{err} = \left(\mathtt{err}^2_{\text{stoch}} + \mathtt{err}^2_{\text{phy}}\right)^{1/2},$$

and an indicator for the total error can be defined as

$$\mathtt{err}_{\text{est}} := (\mathtt{err}^2_{\text{stochest}} + \mathtt{err}^2_{\text{phyest}})^{1/2}, \tag{3.14}$$

where $\mathtt{err}_{\text{stochest}}$ and $\mathtt{err}_{\text{phyest}}$ are defined in (3.9) and (3.13).

Combining the above adaptive procedures for both stochastic and physical approximations, our overall adaptive hybrid spectral strategy processes as follows. First, for a given overall tolerance TOL, we set the initial gPC order to be one (i.e., $q = 1$), and use a very coarse grid to initially partition the physical domain. Then, we compute the numerical approximation $u_{\text{ap}}(\boldsymbol{x}, \boldsymbol{\xi})$ (see (2.6)), and the indicators $\mathtt{err}_{\text{phyest}}$, $\mathtt{err}_{\text{stochest}}$ and $\mathtt{err}_{\text{est}}$ by using (3.9) and (3.13)–(3.14). If the error indicator has a large value, i.e., $\mathtt{err}_{\text{est}} > \mathtt{TOL}$, the solution is refined as follows: if the stochastic approximation error is dominant, i.e., $\mathtt{err}_{\text{stochest}} > \mathtt{err}_{\text{phyest}}$, the the gPC order q needs to be updated by setting $q = q + 1$; if the physical approximation error is important, i.e., $\mathtt{err}_{\text{stochest}} \leq \mathtt{err}_{\text{phyest}}$, the physical mesh T needs to be refined by Algorithm 3.1. This procedure is repeated until $\mathtt{err}_{\text{est}} \leq \mathtt{TOL}$. Algorithm 3.2 gives details of this adaptive hybrid spectral method.

4. Numerical studies

4.1. Test problem 1 (square domain)

In this test problem, we set $D = [-1, 1] \times [-1, 1]$, $\partial D_{\text{D}} = \partial D$, $\partial D_{\text{R}} = \emptyset$, and the source term in (2.1) is specified as

$$f(\boldsymbol{x}) = 2(0.5 - x_1^2 - x_2^2),$$

where $\boldsymbol{x} = [x_1, x_2]^T$.

Algorithm 3.2 The adaptive hybrid spectral method (AHSM)

Set the tolerance TOL, let $q = 1$ and initialize the mesh T.
Compute the numerical solution $u_{\text{ap}}(\boldsymbol{x}, \boldsymbol{\xi})$ in (2.6).
Compute $\texttt{err}_{\text{phyest}}$, $\texttt{err}_{\text{stochest}}$ and $\texttt{err}_{\text{est}}$ by (3.9) and (3.13)–(3.14).
while $\texttt{err}_{\text{est}} > \texttt{TOL}$ **do**
  if $\texttt{err}_{\text{stochest}} > \texttt{err}_{\text{phyest}}$ **then**
    Increase the gPC order, i.e., set $q = q + 1$.
  else
    Set $\epsilon = \texttt{err}_{\text{stochest}}$, and refine the mesh T using Algorithm 3.1.
  end if
  Compute the numerical solution $u_{\text{ap}}(\boldsymbol{x}, \boldsymbol{\xi})$ in (2.6).
  Compute $\texttt{err}_{\text{phyest}}$, $\texttt{err}_{\text{stochest}}$ and $\texttt{err}_{\text{est}}$ by (3.9) and (3.13)–(3.14).
end while

The refractive index in this test problem is set to a truncated Karhunen–Loève (KL) expansion [11, 18] of a random field with mean function $\kappa_0(\boldsymbol{x})$, standard deviation σ and covariance function

$$Cov(\boldsymbol{x}, \boldsymbol{y}) = \sigma^2 \exp\left(-\frac{|x_1 - y_1|}{c} - \frac{|x_2 - y_2|}{c}\right),$$

where $\boldsymbol{x} = [x_1, x_2]^T$, $\boldsymbol{y} = [y_1, y_2]^T$ and c is the correlation length. The KL expansion is expressed as

$$\kappa(\boldsymbol{x}, \boldsymbol{\xi}) = \kappa_0(\boldsymbol{x}) + \sum_{i=1}^{n} \kappa_i(\boldsymbol{x})\xi_i = \kappa_0(\boldsymbol{x}) + \sum_{i=1}^{n} \sqrt{\lambda_i} c_i(\boldsymbol{x})\xi_i,$$

where $\{\lambda_i, c_i(\boldsymbol{x})\}_{i=1}^n$ are eigenpairs of the integral operator associated with $Cov(\boldsymbol{x}, \boldsymbol{y})$, n is the number of KL modes retained, and $\{\xi_i\}_{i=1}^n$ are uncorrelated random variables. When considering Gaussian random fields, the random variables associated with the KL expansion are independent standard normal random variables. However, since the range of Gaussian random fields is unbounded and includes zero, our model problem (2.1)–(2.3) is not well defined if we set $\kappa(\boldsymbol{x}, \boldsymbol{\xi})$ to a Gaussian field. To ensure the well-posedness of our problem, we follow the setting in [12], where the random field is defined through the covariance kernel and the independent uniform random variables with range $[-1, 1]$. In addition, we set $\kappa_0(\boldsymbol{x}) = 4$, $\sigma = 0.2$, $c = 0.625$ and $n = 4$.

To assess the accuracy of the approximation (2.6) based on gPC expansion and the spectral element method, we consider the relative errors of mean and variance functions, which are defined through

$$\texttt{err}_{\text{m}} := \frac{\|\mathbb{E}\left[u_{\text{ap}}\right] - \mathbb{E}\left[u_{\text{ref}}\right]\|_{L^2(D)}}{\|\mathbb{E}\left[u_{\text{ref}}\right]\|_{L^2(D)}},$$
$$\texttt{err}_{\text{v}} := \frac{\|\mathbb{V}\left[u_{\text{ap}}\right] - \mathbb{V}\left[u_{\text{ref}}\right]\|_{L^2(D)}}{\|\mathbb{V}\left[u_{\text{ref}}\right]\|_{L^2(D)}},$$

where u_{ref} is a reference solution.

In this test problem, the reference solution is generated using a non-adaptive hybrid spectral method (NAHSM), where the physical domain is discretized by uniform spectral elements with Lagrange polynomial order $p = 6$ and the stochastic domain is discretized by gPC with order $q = 6$. Moreover, the degrees of freedom of physical domain discretization are $N_{\boldsymbol{x}} = 66049$.

To compare the efficiency of the adaptive hybrid spectral method (AHSM) as in Algorithm 3.2 and the stochastic Galerkin finite element method (SGFEM) where the stochastic domain is discretized by gPC and the physical domain is discretized by low order finite elements (see [31]), we consider the relative errors of mean and variance function estimates with respect to the overall degrees of freedom $\texttt{d.o.f} = N_{\boldsymbol{x}} N_{\boldsymbol{\xi}}$. For AHSM, we set the order of Lagrange interpolation polynomials to $p = 6$ on each physical element, and test seven different values of the tolerance TOL in Algorithm 3.2 ($\texttt{TOL} = 10^{-1}, \ldots, 10^{-7}$). For SGFEM, the physical domain is discretized using the first order rectangular elements, and the gPC order is set to the highest order determined by AHSM, i.e., $q = 5$. To make a further comparison, we also show the results of a non-adaptive hybrid spectral method (NAHSM), where the physical domain is discretized by uniform spectral elements with Lagrange polynomial order $p = 6$ and the stochastic domain is discretized by gPC with order $q = 5$.

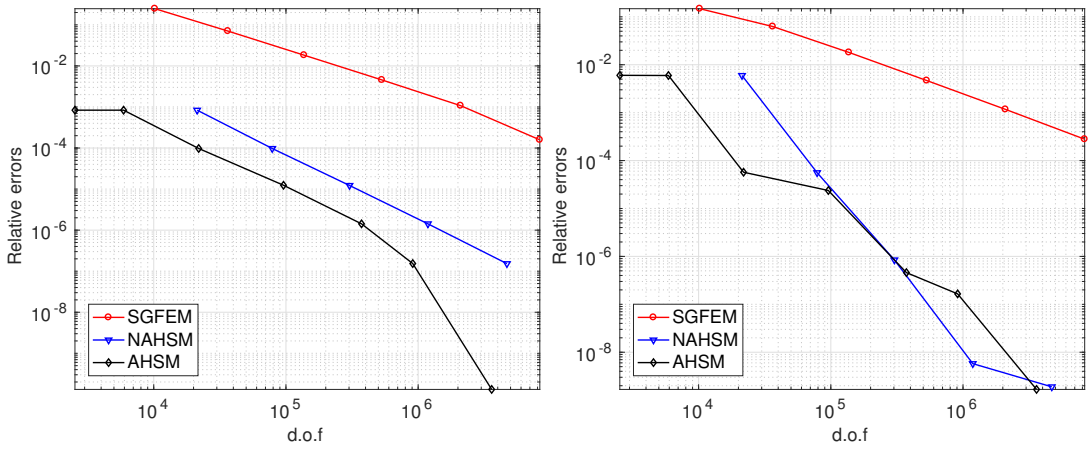

Figure 2: Comparison of the errors of mean (left) and variance (right) functions w.r.t. the overall degrees of freedom.

Figure 2 shows the relative errors of mean (left) and variance (right) functions with respect to the overall degrees of freedom ($\texttt{d.o.f} = N_{\boldsymbol{x}} N_{\boldsymbol{\xi}}$). It is clear that AHSM requires less d.o.f than SGFEM and NAHSM to achieve the same level of accuracy for the mean estimates. For the variance estimates, AHSM and NAHSM require similar d.o.f to achieve accuracies with error smaller than 10^{-4}. It should be noted that, for all our test problems, the magnitudes of the variance estimates are much smaller than the magnitudes of the mean estimates, and therefore the contribution of errors in mean estimates is dominant in the overall error defined in (3.2). This explains why the variance error of AHSM can be larger than that of NAHSM in Figure 2—Algorithm 3.2 conducts adaptively based on the error

indicator for the total error, which may only lead to small errors in its main contribution (the mean error in this test problem). In addition, errors of both AHSM and NAHSM are small compared with SGFEM.

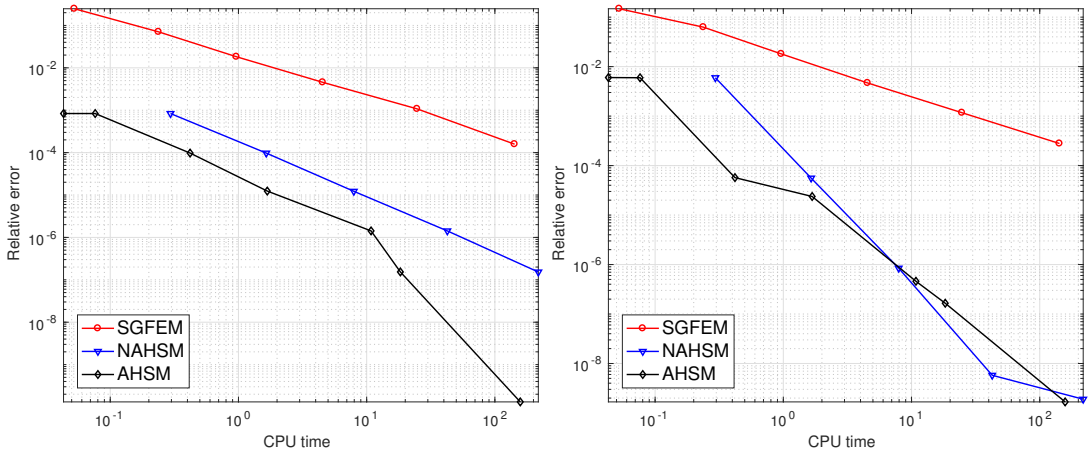

Figure 3: Comparison of the errors of mean (left) and variance (right) functions w.r.t. computation times.

Figure 3 shows errors with respect to the wall clock time for this test problem. The linear system (2.7) is solved by the biconjugate gradient stabilized method (BiCGSTAB) with the mean-based preconditioner [31] in all our test problems, and the computation times refer to the times (wall clock time) spent in BiCGSTAB iterations. It is clear that for a given computation time, AHSM has the smallest error in mean estimates. For the variance estimates, when the computation time is smaller than one, the error of AHSM is smaller than the errors of SGFEM and NAHSM, while the errors of AHSM and SGFEM becomes closer when the computation time becomes larger. In addition, for a given computation time, errors of AHSM and NAHSM in both mean and variance estimates are smaller than the errors of SGFEM.

We also compare the indicators of the total error (3.14) with the errors of mean and variance functions in Figure 4(a) for AHSM. It can be seen that values of the indicator are consistent with the errors of mean and variance functions, and their magnitudes are at the same level. The physical error $\mathtt{err}_{\text{phy}}$ and its indicator $\mathtt{err}_{\text{phyest}}$, and the stochastic error $\mathtt{err}_{\text{stoch}}$ and its indicator $\mathtt{err}_{\text{stochest}}$ are compared in Figure 4(b). Note that the physical and stochastic errors are defined in (3.2)–(3.5) and computed via replacing the solution $u(\boldsymbol{x},\boldsymbol{\xi})$ by the reference solution $u_{\text{ref}}(\boldsymbol{x},\boldsymbol{\xi})$. Form the figure, we can see that the physical and stochastic errors are both consistent with their indicators.

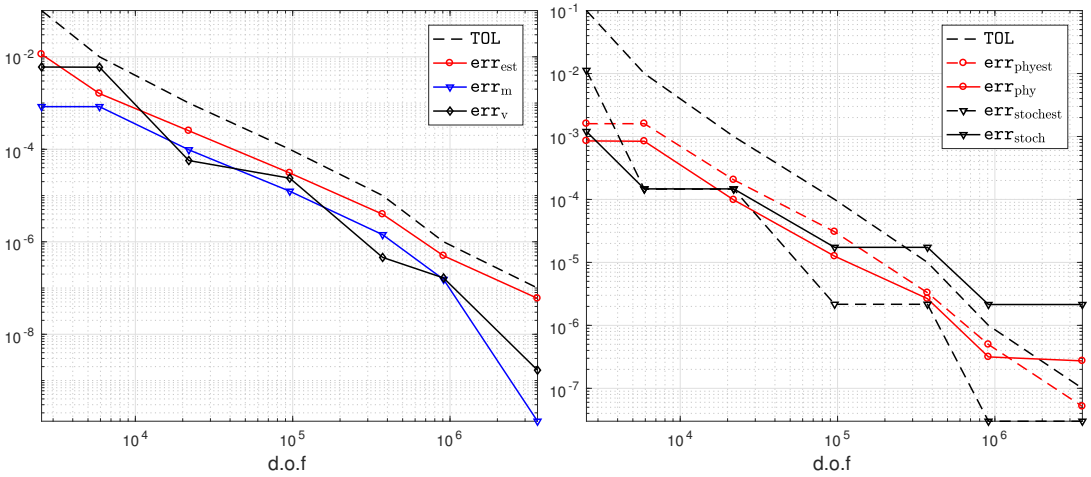

Figure 4: Comparison of the indicators and the errors of mean and variance functions (left), and comparison of the indicators and the physical and stochastic approximation errors (right).

4.2. Test problem 2 (L-shaped domain)

In this problem, the refractive index is set to

$$\kappa(x,\xi) = 1 + 0.3 \cdot \sum_{k=1}^{4} \frac{\cos(kx)\sin(ky)}{k^2}\xi_k,$$

and the force term is the same as that in test problem 1. The physical domain is $D = [-1,1]\times[-1,1]/(-1,0)\times(-1,0)$. The boundary conditions are set to $\partial D_{\mathrm{D}} = \{1\}\times[-1,1]$ and $\partial D_{\mathrm{R}} = \partial D/\partial D_{\mathrm{D}}$.

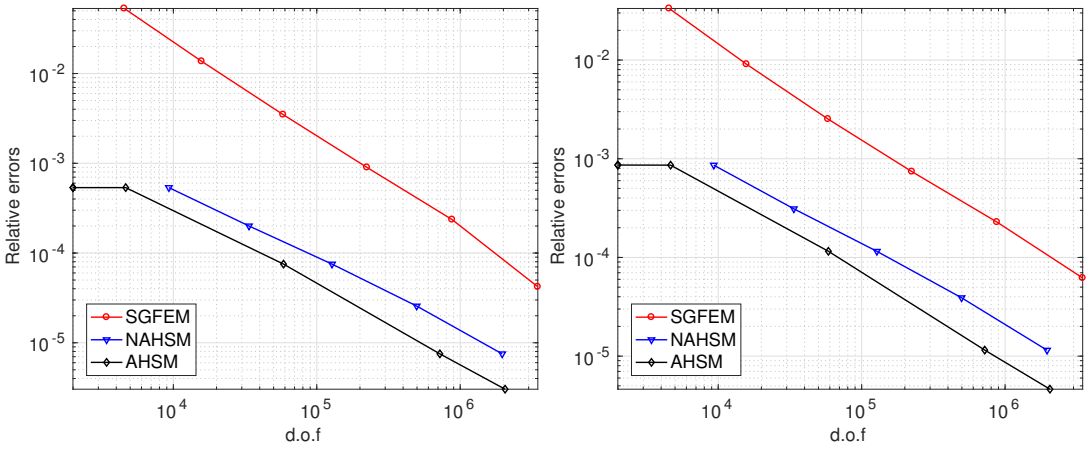

Figure 5: Comparison of the errors of mean (left) and variance (right) functions w.r.t. the overall degrees of freedom.

In this test problem, the reference solution is generated using NAHSM, where the physical domain is discretized by uniform spectral elements with Lagrange polynomial order $p = 6$ and the stochastic domain is discretized by gPC with order $q = 5$. Moreover, the degrees of freedom of physical domain discretization are $N_{\boldsymbol{x}} = 111361$.

To compare the efficiency of AHSM, NAHSM and SGFEM, we show the relative errors of mean and variance functions with respect to the overall degrees of freedom (`d.o.f` $= N_{\boldsymbol{x}} N_{\boldsymbol{\xi}}$) in Figure 5. For AHSM, we set $p = 6$ on each element, and test five different values of the tolerance `TOL` in Algorithm 3.2 (`TOL` $= 10^{-2}, \ldots, 10^{-6}$). For NAHSM, the physical domain is discretized by uniform spectral elements with Lagrange interpolation polynomial order $p = 6$ and the stochastic domain is discretized by gPC with order $q = 4$ (the highest order determined by AHSM for this test problem). For SGFEM, the physical space is discretized by the first order rectangular elements, and the stochastic domain is discretized by gPC with order $q = 4$. From Figure 5, it is clear that AHSM requires less `d.o.f` than SGFEM and NAHSM to achieve a same level of accuracy for both mean and variance estimates.

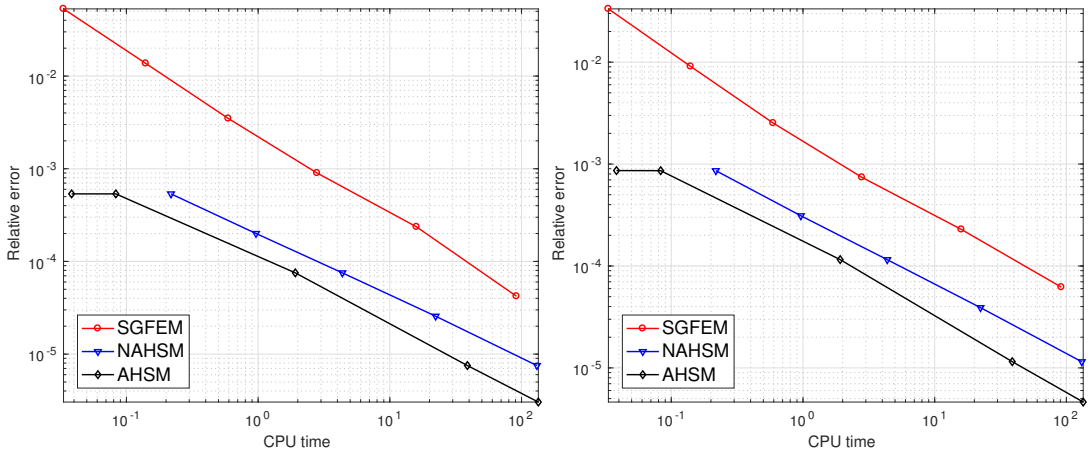

Figure 6: Comparison of the errors of mean (left) and variance (right) functions w.r.t. computation times.

Figure 6 shows errors with respect to computation times for this test problem. It is clear that to achieve an accuracy in mean and variance estimates, AHSM requires less computation times than NAHSM and SGFEM.

Values of the indicator for the total error (3.14) are compared with the errors of mean and variance functions in Figure 7(a) for this test problem. It can be see again that values of the indicator are consistent with the errors of mean and variance functions, and they have the same order of magnitude. We also compare the physical error $\mathtt{err}_{\text{phy}}$, the stochastic error $\mathtt{err}_{\text{stoch}}$ and their indicators in Figure 4(b). Form the figure, we can see that the physical and stochastic errors are both consistent with their indicators.

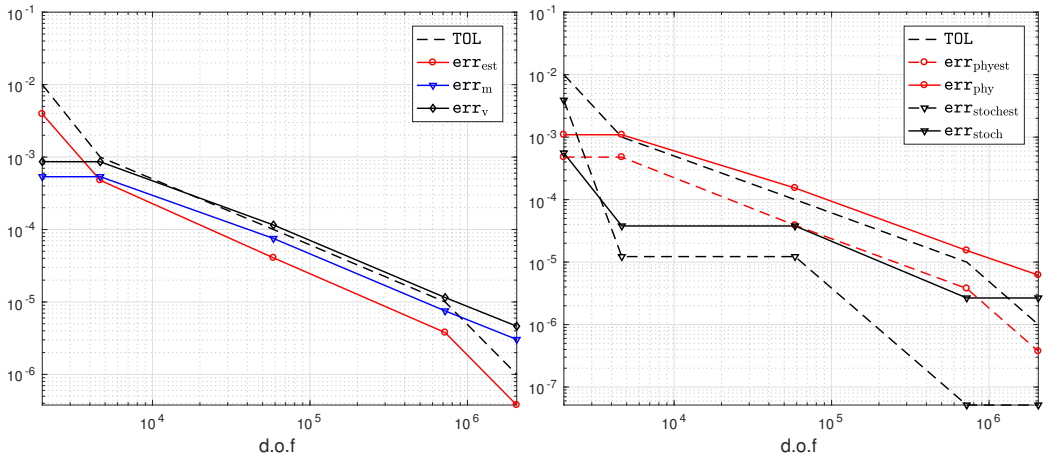

Figure 7: Comparison of the indicators and the errors of mean and variance functions (left), and comparison of the indicators and the physical and stochastic approximation errors (right).

5. Conclusions

Conducting adaptivity is a fundamental concept of efficient numerical methods for solving stochastic PDEs. With a focus on the stochastic Helmholtz equations, our main conclusion is the adaptive hybrid spectral method proposed in this work provides an efficient systematic strategy for solving practical acoustic and optical problems. Our numerical results make it clear that our innovative error indicators provide effective estimates for both stochastic and physical approximation errors, and this new adaptive method requires less overall degrees of freedom than standard adaptive stochastic Galerkin finite element methods to achieve a same level of accuracy. The main limitation of this new method is that its associated linear system is denser than that of the stochastic Galerkin finite element methods, as it is a spectral method for both stochastic and physical approximations. However, since the matrices associate with our method is still blockwise sparse, efficient solvers for stochastic Galerkin finite elements, e.g., block-diagonal preconditioning schemes, can be directly applied for these matrices. Specialized linear solvers for our adaptive hybrid spectral method will be reported in a future paper.

Acknowledgments

This work is supported by the National Natural Science Foundation of China (No. 11601329) and the science challenge project (No. TZ2018001).

References

[1] I. Babuška, R. L. Tempone, G. E. Zouraris, *Galerkin finite element approximations of stochastic elliptic partial differential equations*, SIAM Journal on Numerical Analysis, 42 (2004), pp. 800–825.

[2] A. BESPALOV, C. E. POWELL, D. SILVESTER, *Energy norm a posteriori error estimation for parametric operator equations*, SIAM Journal on Scientific Computing, 36 (2014), pp. A339–A363.
[3] A. BESPALOV, D. SILVESTER, *Efficient adaptive stochastic galerkin methods for parametric operator equations*, SIAM Journal on Scientific Computing, 38 (2016), pp. A2118–A2140.
[4] D. BRAESS, *Finite Elements*, Cambridge University Press, London, 1997.
[5] Y. CAO, R. ZHANG, K. ZHANG, *Finite element and discontinuous Galerkin method for stochastic Helmholtz equation in two-and three-dimensions*, Journal of Computational Mathematics, 28 (2008) pp. 702–715.
[6] M. CHENG, T.Y. HOU AND Z. ZHANG, *A dynamically bi-orthogonal method for time-dependent stochastic partial differential equations I: Derivation and algorithms*, J. Comput. Phys., 242 (2013), pp. 843–868.
[7] M. CHENG, T.Y. HOU AND Z. ZHANG, *A dynamically bi-orthogonal method for time-dependent stochastic partial differential equations II: Adaptivity and generalizations*, J. Comput. Phys., 242 (2013), pp. 753–776.
[8] Y. CHEN, S. GOTTLIEB, *Reduced collocation methods: Reduced basis methods in the collocation framework*, Journal of Scientific Computing, 55 (2013), pp. 718–737.
[9] M.K. DEB, I.M. BABUŠKA AND J.T. ODEN, *Solution of stochastic partial differential equations using Galerkin finite element techniques*, Comput. Methods Appl. Mech. Engrg., 190 (2001), pp. 6359–6372.
[10] M. EIGEL, C. GITTELSON, C. SCHWAB, E. ZANDER, *Adaptive stochastic Galerkin FEM*, Computer Methods in Applied Mechanics and Engineering, 270 (2014), pp. 247–269.
[11] H. ELMAN, D. FURNIVAL, *Solving the stochastic steady-state diffusion problem using multigrid*, IMA Journal of Numerical Analysis, 27 (2007), pp. 675–688.
[12] H. C. ELMAN, C. W. MILLER, E, T. PHIPPS AND R. S. TUMINARO, *Assessment of collocation and Galerkin approaches to linear diffusion equations with random data*, International Journal for Uncertainty Quantification, 1 (2011), pp. 19–33.
[13] H. C. ELMAN, D. J. SILVESTER, A. J. WATHEN, *Finite elements and fast iterative solvers: with applications in incompressible fluid dynamics*, Oxford University Press (UK), 2014.
[14] Z. FANG, J. LI, T. TANG AND T. ZHOU, *Efficient stochastic Galerkin methods for Maxwell's equations with random input*, J. Sci. Comput., 80 (2019), pp. 248–2267.
[15] X. FENG, J. LIN, C. LORTON, *An efficient numerical method for acoustic wave scattering in random media*, SIAM/ASA Journal on Uncertainty Quantification, 3 (2015), pp. 790–822.
[16] A. FROLOV AND E. KARTCHEVSKIY, *Integral equation methods in optical waveguide theory*, in: *Inverse Problems and Large-Scale Computations*, Springer (2013) , pp. 119–133.
[17] R.G. GHANEM AND R.M. KRUGER, *Numerical solution of spectral stochastic finite element systems*, Comput. Methods Appl. Mech. Engrg., 129 (1996), pp. 289–303.
[18] R. G. GHANEM, P. D. SPANOS, *Stochastic finite elements: a spectral approach*, Courier Corporation, 2003.
[19] F. IHLENBURG, I. BABUŠKA, *Finite element solution of the Helmholtz equation with high wave number part I: The h-version of the FEM*, Computers & Mathematics with Applications, 30 (1995), pp. 9–37.
[20] F. IHLENBURG, I. BABUŠKA, *Finite element solution of the Helmholtz equation with high wave number part II: the hp version of the fem*, SIAM Journal on Numerical Analysis, 34 (1997), pp. 315–358.
[21] F. B. JENSEN, W. A. KUPERMAN, M. B. PORTER, H. SCHMIDT, *Computational ocean acoustics*, Springer Science & Business Media, 2011.
[22] E. KARCHEVSKII AND S. SOLOV'EV, *Investigation of a spectral problem for the Helmholtz operator on the plane*, Differ. Equ., 36 (2000), pp. 631–634.

[23] E. KARTCHEVSKI, A. NOSICH AND G. HANSON, *Mathematical analysis of the generalized natural modes of an inhomogeneous optical fiber*, SIAM J. Appl. Math., 65 (2005), pp. 2033–2048.
[24] R. MÄRZ, *Integrated optics: design and modeling*, Artech House on Demand, 1995.
[25] C. MAVRIPLIS, *Adaptive mesh strategies for the spectral element method*, Computer Methods in Applied Mechanics & Engineering, 116 (1994), pp. 77–86.
[26] W. F. MITCHELL, M. A. MCCLAIN, *A Survey of hp-Adaptive Strategies for Elliptic Partial Differential Equations*, Springer Netherlands, 2011.
[27] E. MUSHARBASH, F. NOBILE AND T. ZHOU, *Error analysis of the dynamically orthogonal approximation of time dependent random PDEs*, SIAM J. Sci. Comput., 37 (2015), pp. A776–A810.
[28] J. LI, P. STINIS, *Mesh refinement for uncertainty quantification through model reduction*, Journal of Computational Physics, 280 (2015), pp. 164–183.
[29] J. LI, P. STINIS, *A unified framework for mesh refinement in random and physical space*, Journal of Computational Physics, 323 (2016), pp. 243–264.
[30] A. T. PATERA, *A spectral element method for fluid dynamics: Laminar flow in a channel expansion*, Journal of Computational Physics, 54 (1984), pp. 468–488.
[31] C. E. POWELL, H. C. ELMAN,*Block-diagonal preconditioning for spectral stochastic finite-element systems*, IMA Journal of Numerical Analysis, 29 (2009), pp. 350–375.
[32] J. SHEN, T. TANG, *Spectral and High-Order Methods with applications*, Science Press, 2006.
[33] L. N. TREFETHEN, *Approximation Theory and Approximation Practice*, Society for Industrial and Applied Mathematics, 2013.
[34] L. TREFETHEN, *Multivariate polynomial approximation in the hypercube*, Proceedings of the American Mathematical Society, 145 (2017), pp. 4837–4844.
[35] FN VAN DE VOSSE, P. D, MINEV, *Spectral element methods: theory and applications*, Eindhoven University of Technology, 1996.
[36] X. WAN, G. E. KARNIADAKIS, *An adaptive multi-element generalized polynomial chaos method for stochastic differential equations*, Journal of Computational Physics, 209 (2005), pp. 617–642.
[37] D. XIU, G. E. KARNIADAKIS, *Modeling uncertainty in steady state diffusion problems via generalized polynomial chaos*, Computer Methods in Applied Mechanics and Engineering, 191 (2002), pp. 4927–4948.
[38] D. XIU AND G.E. KARNIADAKIS, *Modeling uncertainty in flow simulations via generalized polynomial chaos*, J. Comput. Phys., 187 (2003), pp. 137–167.
[39] D. XIU, *Numerical methods for stochastic computations: a spectral method approach*, Princeton University Press, 2010.
[40] D. XIU, G. E. KARNIADAKIS, *The wiener–askey polynomial chaos for stochastic differential equations*, SIAM journal on scientific computing, 24 (2002), pp. 619–644.
[41] D. XIU, J. SHEN, *Efficient stochastic galerkin methods for random diffusion equations*, Journal of Computational Physics, 228 (2009), pp. 266–281.
[42] C. VASSALLO, *Optical waveguide concepts*, Elsevier, 1991.
[43] T. TANG AND T. ZHOU, *Convergence analysis for stochastic collocation methods to scalar hyperbolic equations*, Commun. Comput. Phys., 8 (2010), pp. 226–248.
[44] T. ZHOU AND T. TANG, *Galerkin methods for stochastic hyperbolic problems using bi-orthogonal polynomials*, J. Sci. Comput., 51 (2012), pp. 274-292.